Analysis of Wireless Power Transfer Efficiency and Specific Absorption Rate for a Distributed Brain Implant System

Julian Alonzo[1], Marinus H. Daling[1], Jihun Lee[2], Ah-Hyoung Lee[2],
David Durfee[2], Peter Asbeck[3], Lawrence Larson[2], Arto Nurmikko[2], Vincent W. Leung[1]

[1]Baylor University, Waco, TX, USA
[2]Brown University, Providence, RI, USA
[3]University of California, San Diego, La Jolla, CA, USA

2024 IEEE 20th International Conference on Body Sensor Networks (BSN) | 979-8-3315-3014-3/24/$31.00 ©2024 IEEE | DOI: 10.1109/BSN63547.2024.10780624

***Abstract*— Wireless sub-mm sized distributed brain implants have been proposed as the next frontier of Brain-Machine Interface (BMI) design to achieve untethered, high-density neural recording and stimulation. Simultaneously improving the wireless power transfer (WPT) efficiency and reducing the specific absorption rate (SAR) will be crucial for its clinical success. Towards these goals, we present an EM simulation method, a lumped equivalent circuit model, and a theoretical analysis to accurately predict the power delivered to the recording/ stimulating nodes, as well as the power dissipated in biological tissues and all other lossy elements within the system. This comprehensive framework also explains how increasing the distance between the transmit coil and the scalp can beneficially reduce the SAR without undermining the WPT efficiency. This work presents a rigorous prediction technique for transmission loss and tissue heating towards performance optimization.**

Keywords*— *Wireless biomedical implants, brain-machine interface, wireless power transfer, specific absorption rate.

I. Introduction

Brain-Machine interfaces (BMI) based on electrocorticography (ECoG) microelectrode arrays have been successfully transitioned in many human clinical trials. Scaling up to provide many thousands of flexibly re-configurable, densely populated neural nodes is the next frontier for BMI research. Various teams of researchers have proposed sub-mm sized distributed wireless implants to address this challenge [1-9]. Each of the implants, which operate independently from one another, features dedicated analog neural frontends for recording and/ or stimulation as well as circuits for energy harvesting and data communication. Some of these systems achieve wireless power transfer (WPT) by near-field inductive coupling [1,3,5,6,9], where an external transmit (Tx) coil is used to wirelessly transfer energy to the receive coil (Rx) at each recording/stimulating node. To protect against excessive temperature rise in the body, the localized exposure shall not result in a peak Specific Absorption Rate (SAR) that exceeds 10 W/kg (averaged over any 10 g of tissue) [10].

This paper focuses on the WPT and SAR analysis of the distributed brain implant system of [6], but the methodologies and insights are appliable to other wireless BMI as well as biomedical implant systems in general.

Fig. 1(a) shows the 3-layer WPT system evaluated in this study. Operating at 915 MHz, it is composed of: (i) a Tx coil external to the head, (ii) a relay coil implanted on the cortex, and (iii) micro Rx-coils integrated on an ensemble of neural nodes

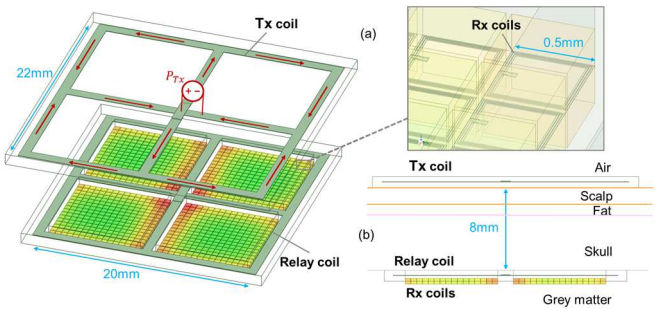

Fig. 1. (a) 3-layer inductively coupled "Neurograin" system. (b) Cross-section showing 8mm of tissue separation between the Tx and the relay coils

(IC chips). Each chip - known as a "Neurograin" - measures 0.5 × 0.5 mm^2. It comprises an RF rectifier for energy-harvesting, as well as all RF/ analog circuits for uplink/ downlink communication and neural sensor/ stimulator functions.

As shown in Fig. 1(b), tissue (scalp, fat, skull) thickness of 8 mm, which denotes the minimum separation distance of the Tx and the relay coils, is assumed. The Tx and the relay coils, each measuring 22 × 20 mm^2, are designed with a 4-quadrant geometry to optimize the magnetic field intensity over the covered area [6]. Each quadrant is capable of accommodating an Neurograin array as large as 16 × 16 (= 256). As a result, up to 1024 nodes can be supported with the current configuration.

An important design consideration of the WPT system is the inevitable spatial non-uniformity of the magnetic field strength. The most weakly coupled implants (those at the center of a quadrant) dictate the required external Tx power, while the more strongly coupled implants (those along the edges) will receive higher incident power. Under extreme conditions, unless over-voltage protection (OVP) is featured to limit the rectified voltages, transistor breakdown could occur.

This work assumes that OVP is achieved through on-chip "auto-tuning" [11], in which a programmable capacitor bank at the input is automatically de-tuned (i.e., the LC resonance frequency is appropriately shifted above 915 MHz) to reject excessive RF input power. As revealed by circuit simulations and theoretical analysis, the approach achieves better WPT efficiency than the more conventional "clamps OVP" [11], so lower Tx power is required and the SAR is correspondingly improved.

This study extends the analysis of [11], which calculates the WPT efficiency from the RF source to chip loads, to

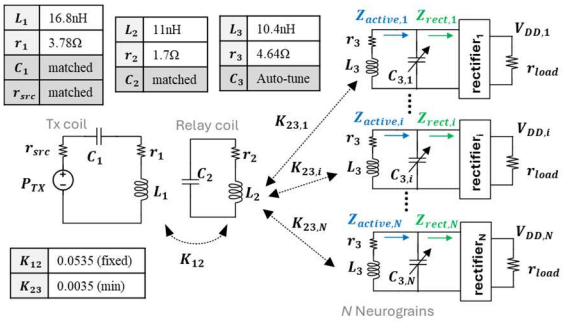

Fig. 2. Equivalent lumped circuit model of the 3-layer WPT system.

systematically determine the power dissipated in brain tissues and all other lossy circuit elements. We will explain why a moderate increase of the distance between the Tx coil and the scalp can significantly lower the SAR field while maintaining the WPT efficiency. This work presents a rigorous prediction technique for transmission loss and tissue heating – as well as a methodology for performance optimization – for a distributed network of wirelessly powered biomedical implants.

This paper is organized as follows. Section II discusses the EM simulation of the 3-layer inductive coupling system, and how it can be extracted to build an equivalent (lumped) circuit model. Section III precisely calculates the power distribution throughout the network. Section IV presents the SAR simulation and analysis. A summary is given in Section V.

II. EM Simulation and Circuit Modeling of the Distributed Neurograin WPT System

The 3-layer WPT system of Fig. 1 is modelled in Ansys HFSS. Simulations are run to determine the 3-port (one port for each of the three coils) Z-parameters at 915 MHz, which will be post-processed to extract the lumped circuit parameters for calculation purposes. As a result, the rather involved distributed WPT physical structure is conveniently turned into a lumped equivalent circuit as shown in Fig. 2, where L_1, L_2, L_3 (and r_1, r_2, r_3) represent the inductances (and the lossy components) of the Tx, relay and on-chip coils, respectively. Furthermore, K_{12} represents the (fixed) coupling coefficient between the Tx and the relay coils. $K_{23,i}$ denotes the location-dependent coupling coefficient between the relay and the Rx coil of the i-th Neurograin, capturing the non-uniform magnetic field strength across the array.

To determine the $K_{23,i}$ variation, the simulation process was automated to sweep the Neurograin location across one quadrant (16 × 16 array) of the relay coil. Fig. 3(a) plots the simulated $K_{23,i}$ on the array, illustrating the non-uniform magnetic field

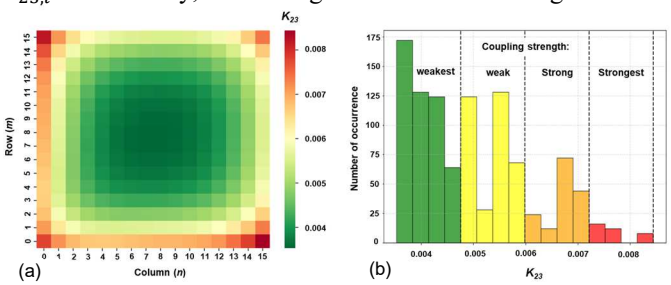

Fig. 3. (a) K_{23} over a 16×16 array (i.e., one-quadrant of the relay coil), and (b) Distribution of K_{23} over all four quadrants of the relay coil.

"heat map". As predicted, Neurograins at the center (farthest from the relay coil) have the smallest coupling coefficients, while those near the edge/ at the corner have the largest. The maximum coupling coefficient is roughly 2.5× larger than the minimum one. Fig. 3(b) re-plots the simulated $K_{23,i}$ results in a histogram, highlighting its distribution. Since results from the other 3 quadrants are identical because of physical symmetry, we simply multiply the number of occurrence by four. For ease of subsequent circuit analysis, we further apply a simple "4-tier" distribution as shown in Table I. Also shown are the tuned capacitance ($C_{3,i}$) values to achieve the appropriate OVP.

TABLE I. "4-Tier" Coupling Coefficents ($K_{23,i}$) and Distribution

Coupling Strength	$K_{23,i}$	No. of nodes (Total = N)	Tuned $C_{3,i}$ (for OVP)
Strongest	$2.5 \cdot K_{23min}$	$0.1 \cdot N$	1.5 pF
Strong	$2 \cdot K_{23min}$	$0.1 \cdot N$	1.8 pF
Weak	$1.5 \cdot K_{23min}$	$0.3 \cdot N$	2.1 pF
Weakest	K_{23min}	$0.5 \cdot N$	2.7 pF

Using parameters given in Fig. 2 and Table I, transistor-level circuit simulations are used to study the WPT system and verify the theoretical analysis. For example, Fig. 4 shows the simulated Tx power (P_{Tx}) required to energize varying number of nodes, based on the parameters extracted from HFSS.

Before we proceed with a theoretical analysis, we shall examine the nature of r_1, r_2, and r_3. These lossy components are caused by the resistivity of the coils themselves (r_{ohmic}), as well as the eddy current losses induced in the nearby brain tissues (r_{tissue}). One can write:

$$r_1 = r_{1,ohmic} + r_{1,tissue} \quad (1)$$

Similar equations also apply to r_2, and r_3. To differentiate the so-called "ohmic" and "tissue" components, we repeat our HFSS simulation without any biological tissues (i.e., coils are suspended in air), and the extracted r_1 would then equal $r_{1,ohmic}$. Understandably, the simulated inductances also increase slightly (by <10%), which can be neglected.

Table II shows the decomposition for r_1, r_2, and r_3. For the Tx and relay coils, the majority of the loss is due to eddy currents induced in surrounding tissues (or tissue heating). For the Neurograin (chip) coils, which have much smaller size and thickness, the opposite is true.

TABLE II. Decomposition of Coil Resistance

Resistance	Tx coil	Relay coil	Chip coil
Total, r (Ω)	3.78	1.7	4.64
r_{ohmic} (Ω)	0.31	0.17	4.6
r_{tissue} (Ω)	3.47	1.53	0.05

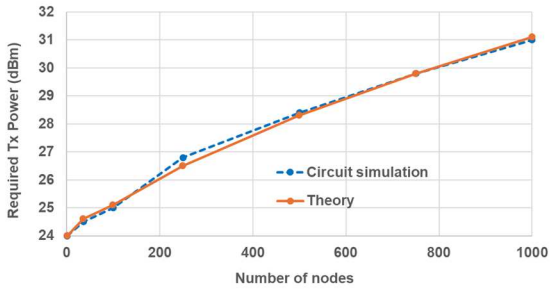

Fig. 4. Required P_{Tx} versus number of nodes in the WPT sytsem

III. Analysis of Power Distribution in the WPT System

In this section, we will present an analytical framework to eventually calculate the "useful" wireless power delivered to the Neurograin loads, and the power "wasted" on various lossy components. We believe this will greatly assist any WPT and SAR co-optimization, as will be demonstrated in the next section.

In general, when two inductors (L_a, L_b) are linked by their mutual inductance (M_{ab}), and the secondary inductor L_b is terminated by a series load Z_b $(= R_b - j/(\omega C_b))$, it can be shown that an impedance Z_{ref} $(= R_{ref} + jX_{ref})$ is reflected to the primary side according to [12]:

$$Z_{ref} = \frac{\omega^4 C_b^2 R_b M_{ab}^2}{(1-\omega^2 L_b C_b)^2+(\omega C_b R_b)^2} + j\frac{\omega^3 C_b(1-\omega^2 L_b C_b)M_{ab}^2}{(1-\omega^2 L_b C_b)^2+(\omega C_b R_b)^2} \quad (2)$$

Using a harmonic-balance (HB) circuit simulator, we can find the impedances, such as $Z_{rect,i}$ and $Z_{active,i}$ of Fig. 2, at the interfaces between the Neurograin coils and the rectifiers. They are shown in Table III. Note that $Z_{active,i}$ is composed of $Z_{rect,i}$ and the impedance of the tuning capacitor (where the values of $C_{3,i}$ are given in Table I). In this analysis, we further assume the switched-C network has a moderate quality factor of 12 ($Q = 1/(\omega C_{3,i} r_{sw,i})$, where $r_{sw,i}$ denotes the series switch on-resistance). The imaginary part of $Z_{active,i}$ is dominated by the impedance of $C_{3,i}$.

TABLE III. Calculated Reflected Impedances for the WPT system

Coupling strength		Strongest	Strong	Weak	Weakest
No. of nodes (total = 1000)		100	100	300	500
HB sim: Neurograin Impedances	$R_{rect,i}$ (Ω)	1.35	1.02	0.78	0.51
	$R_{active,i}$ (Ω)	8.3	7.2	6.4	5
	$X_{active,i}$ (Ω)	-95.8	-83.5	-73.1	-58.8
Calculation: Reflected Impedances on L_2 and L_1	$\Sigma R_{ref,L2,i}$ (Ω)	0.23	0.28	1.02	2.33
	$\Sigma X_{ref,L2,i}$ (Ω)	0.68	0.59	1.34	0.02
	$R_{ref,L1}$ (Ω)	2.26			
	$X_{ref,L1}$ (Ω)	0.007			

Using (2), we can write down the reflected impedance on the relay coil $(Z_{ref,L2,i})$ as follows:

$$R_{ref,L2,i} = \frac{\omega^4 C_{node,i}^2 R_{node,i} M_{23,i}^2}{(1-\omega^2 L_3 C_{node,i})^2+(\omega C_{node,i} R_{node,i})^2} \quad (3)$$

$$X_{ref,L2,i} = \frac{\omega^3 C_{node,i}(1-\omega^2 L_3 C_{node,i})M_{23,i}^2}{(1-\omega^2 L_3 C_{node,i})^2+(\omega C_{node,i} R_{node,i})^2} \quad (4)$$

where $M_{23,i} = K_{23,i}\sqrt{L_2 L_3}$, $R_{node,i} = r_3 + R_{active,i}$, and $C_{node,i} = -1/(\omega X_{active,i})$, respectively.

Similarly, the reflected impedance on the Tx coil $(Z_{ref,L1})$ are given by:

$$R_{ref,L1} = \frac{\omega^4 C_{relay,tot}^2 R_{relay,tot} M_{12}^2}{(1-\omega^2 L_2 C_{relay,tot})^2+(\omega C_{relay,tot} R_{relay,tot})^2} \quad (5)$$

$$X_{ref,L1} = \frac{\omega^3 C_{relay,tot}(1-\omega^2 L_2 C_{relay,tot})M_{12}^2}{(1-\omega^2 L_2 C_{relay,tot})^2+(\omega C_{relay,tot} R_{relay,tot})^2} \quad (6)$$

where $M_{12} = K_{12}\sqrt{L_1 L_2}$, $R_{relay,tot} = r_2 + \sum_{i=1}^{N} R_{ref,L2,i}$, and $C_{relay,tot} = -1/[\sum_{i=1}^{N}(\omega X_{ref,L2,i}) - 1/C_2]$, respectively.

Table III summarizes these reflected impedances. The overall WPT equation for the i^{th} Neurograin is given by a product of efficiency terms ($P_{TX} \cdot \eta_1 \cdot \eta_2 \cdot \eta_3 \cdot \eta_{rect} = P_{L,i}$):

$$P_{TX} \cdot \frac{R_{ref,L1}}{R_{ref,L1}+r_1+r_{src}} \cdot \frac{R_{ref,L2,i}}{\sum_{i=1}^{N} R_{ref,L2,i}+r_2} \cdot \frac{R_{rect,i}}{R_{active,i}+r_3} \cdot \eta_{rect} = P_{L,i} \quad (7)$$

where $P_{L,i}$ is the DC load power (on r_{load}, at 20 uW) on the i^{th} node, and η_{rect} is the rectifier RF-to-DC efficiency (found to be ~70% [6]). As shown in Fig. 4, the calculated required P_{TX} agrees well with that obtained by simulation, thus confirming our analysis.

Using this framework, we can account for all the power dissipated in the WPT system. For example, the power lost to tissues through L_1 and L_2 are readily given by:

$$P_{r1,tissue} = P_{Tx} \cdot \frac{r_{1,tissue}}{R_{ref,L1}+r_1+r_{src}} \quad (8)$$

$$P_{r2,tissue} = P_{Tx} \cdot \eta_1 \cdot \frac{r_{2,tissue}}{\sum_{i=1}^{N} R_{ref,L2,i}+r_2} \quad (9)$$

Similar equations can be derived to calculate the power wasted as resistive heating of the Tx, relay and all Neurograin coils ($P_{r1,ohmic}$, $P_{r2,ohmic}$, and $P_{r3,ohmic}$), capacitor switch banks (P_{sw}), rectifiers (P_{rect}), as well as the total "useful" power delivered to all Neurograin loads ($P_{load} = \Sigma P_{L,i}$). Fig. 5(a) shows the overall power distribution inside the WPT system. Note that the overall WPT efficiency (defined as P_{load}/P_{Tx}) is about 1%, and the majority of the power (about 66%) is dissipated in brain tissues ($P_{r1,tissue} + P_{r2,tissue}$). The numerous Neurograin micro-coils contribute negligibly to tissue heating, i.e., $\Sigma P_{r3,tissue}$ is insignificant.

Fig. 5(b) shows the calculated power dissipation on brain tissues versus the number of nodes. While all other power categories hold relatively constant, there is a higher percentage of Tx power dissipated on tissue through the Tx coil ($P_{r1,tissue}$) than that through the relay coil ($P_{r2,tissue}$), as the number of nodes increases. While this can be directly explained through the reflected impedances, its implication to SAR field intensity remains to be studied.

IV. SAR Simulation and Analysis

Fig. 6(a) shows the HFSS-simulated SAR results with $P_{Tx} =$ 24 dBm and only one Neurograin node present. The peak SAR reaches 22.3 W/kg at the head tissue closest to the Tx coil.

Recognizing that SAR is closely related to eddy currents induced on the tissue by the Tx coil, we can reduce SAR by introducing a few mm of separation (air gap) between the Tx coil and the head, as shown in Fig. 6(b). According to (8), as $r_{1,tissue}$ reduces, so does the $P_{r1,tissue}$. With a 3 mm air gap, the SAR reduces by 35% to 14.6 W/kg.

While the reduced SAR is not surprising, it is accomplished *without reducing the overall WPT efficiency*. Referring to the η_1 term from (7), which represents the L_1-to-L_2 coupling efficiency:

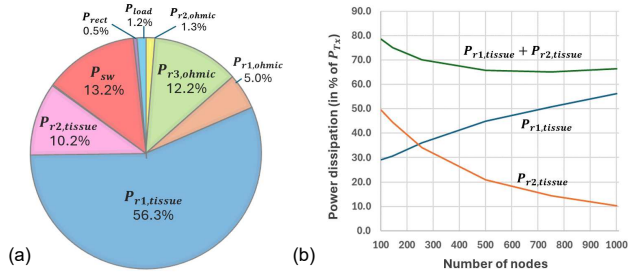

Fig. 5. (a) Breakdown on power dissipation for the 1000-node WPT system. (b) Percentage of power lost to brain tissues vs. the number of nodes .

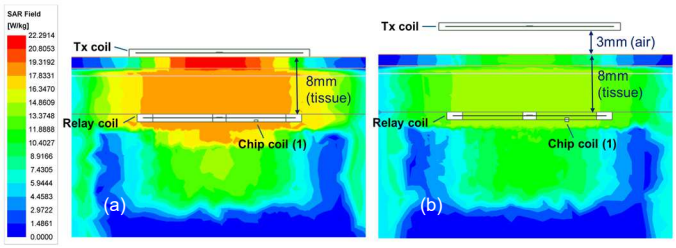

Fig. 6. HFSS-simulated SAR results assuming (a) the default setting shown in Fig. 1(b), and (b) an air gap of 3mm is introduced below the Tx coil.

$$\eta_1 = \frac{R_{ref,L1}}{R_{ref,L1}+r_{1,ohmic}+r_{1,tissue}+r_{src}} \quad (10)$$

As the air gap gradually increases, there exists an optimal distance where the detrimental effects of a reduced $R_{ref,L1}$ (caused by a smaller mutual inductance, $M_{12} = K_{12}\sqrt{L_1 L_2}$) on η_1 can be *compensated* by a reducing $r_{1,tissue}$. Fig. 7(a) plots the calculated η_1 alongside the HFSS-simulated S_{21} (=P_{load}/P_{Tx}), both normalized, versus the air gap distance. Good agreement is observed. We conclude that a gap of 3mm would be very desirable for this particular WPT system. Furthermore, Fig. 7(b) compares the total tissue loss ($P_{tissue} = P_{r1,tissue} + P_{r2,tissue}$) against the simulated SAR results. They follow roughly the same trend, supporting our assumption that the two quantities are closely related.

Our analysis shows that the air gap's SAR and S_{21} benefits also apply to higher number of nodes. When an air gap is introduced such that the P_{tissue} is reduced while S_{21} stays constant (thus requiring the same P_{Tx}), the total Tx power must be distributed differently in the system. Fig. 8 displays the re-calculated power pie chart with 3 mm air gap. Comparing Fig. 8 with Fig. 5(a), the reduction of power dissipated in the tissue (through $P_{r1,tissue}$) now results in a corresponding increase in Tx coil ohmic heating (through $P_{r1,ohmic}$). Since the Tx coil is external to the head, it does not contribute to tissue heating concerns.

Python code are written to populate an array of Neurograins in HFSS and to automatically set the appropriate $Z_{active,i}$ based on the location of each node. Table IV shows the simulated SAR results for up to 256 nodes, along with the calculated P_{tissue} for easy reference. Although total input power (P_{Tx}) is increasing as higher number of nodes are enabled, simulations completed so far indicate a near constant or slightly decreasing SAR field. While the air gap improves the situation, the current system as designed still exceeds the 10W/kg SAR requirements [10]. The

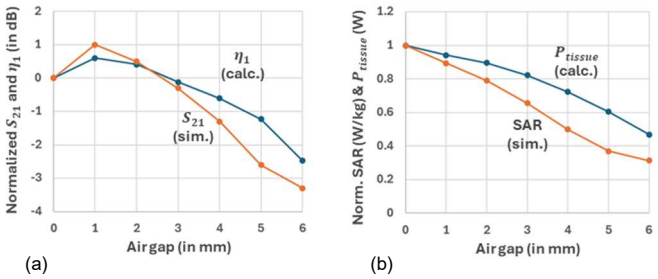

Fig. 7. Effects of Tx-to-scalp air gap. (a) Simulated S_{21} vs calculated η_1. (b) Simulated SAR vs. calculated P_{tissue}. (All quantities are normalized to the corresponding values at 0 mm distance.)

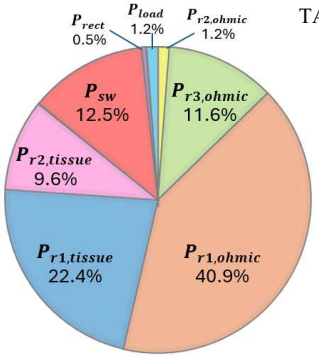

Fig. 8. 1000-node WPT system power distribution with a 3 mm air gap under the Tx coil.

TABLE IV. SIMULATED SAR VERSUS NUMBER OF NEUROGRAIN NODES

No of Nodes	P_{Tx} (dBm)	Sim. SAR (W/kg)	Calc. P_{tissue} (mW)
1	24	14.7	186
16	24	13.5	180
36	24.5	13.3	192
64	24.8	13.1	194
100	25.1	13.8	194
144	25.4	12.9	193
196	25.9	11.5	200
256	26.4	11.8	207
512	28.2	n/a	251
1000	31.1	n/a	404

analysis presented here points the way towards further SAR-conscious, WPT optimized design techniques.

V. SUMMARY

Using a combination of EM simulation and circuit modelling techniques, we demonstrated the calculation of the power distribution on all loads and lossy elements within a inductively-coupled WPT system with a high number (up to 1000) of nodes. Of particular interest is the power dissipated as heat on biological tissues, which is related to the SAR. Using the "Neurograin" BMI design as an example, this analytical framework reveals how a moderate air gap introduced between the external Tx coil and the head can significantly reduce SAR while maintaining WPT efficiency. We believe the analysis methods and design insights are applicable to any inductively powered biomedical implant system.

VI. ACKNOWLEDGEMENTS

This research was supported by NSF/ECCS Grant 2322601.

REFERENCES

[1] M. Maharbiz et al., "Reliable Next-Generation Cortical Interfaces for Chronic Brain–Machine Interfaces and Neuroscience," *Proc. of the IEEE*, Jan. 2017.

[2] D. Piech et al., "Rodent wearable ultrasound system for wireless neural recording," *Int. Conf. IEEE EMBC*, 2017.

[3] Khalifa et al., "The Microbead: A 0.009 mm^3 Implantable Wireless Neural Stimulator," *IEEE Trans. on BioCAS*, Oct. 2019.

[4] J. Lim et al., "A 0.19×0.17mm2 Wireless Neural Recording IC for Motor Prediction with Near-Infrared-Based Power and Data Telemetry," *ISSCC*, 2020.

[5] Y. Jia et al., "A Trimodal Wireless Implantable Neural Interface System-on-Chip," *IEEE Trans. on Biomedical Circuits and Systems*, Dec. 2020.

[6] Lee, J., Leung, V., Lee, AH. et al. Neural recording and stimulation using wireless networks of microimplants. *Nat Electron* 4 (2021).

[7] M. Pola et al., "Galvanic Brain-Coupled Communication Among Freely Floating Micro-Scale Implants," *IEEE BioCAS Conference*, 2023.

[8] J. Lee et al., "A Sub-mm^3 Wireless Neural Stimulator IC for Visual Cortical Prosthesis With Optical Power Harvesting and 7.5-kb/s Data Telemetry," *IEEE JSSC*, Apr. 2024.

[9] G. Barbruni et al., "A Freq-Switching Inductive Power Transfer System for Wireless, Miniaturised and Large-Scale Neural Interfaces," *IEEE Trans. BioCAS*, June 2024.

[10] "IEEE Standard for Safety Levels with Respect to Human Exposure to Radio Frequency EM Fields, 3 kHz to 300 GHz," *IEEE Std C95.1-2005*, Apr. 2006.

[11] V. W. Leung et al., "Improving Wireless Power Transfer Efficiency for Distributed Brain Implants using Auto-Tune OVP," *IEEE BioCAS Conference*, 2023.

[12] D. M. Beams and S. G. Annam, "Validation of a reflected-impedance design method for wireless power transfer applications," *IEEE Int. MWSCAS*, 2012